

Assessment of InSAR Atmospheric Correction Using Both MODIS Near-Infrared and Infrared Water Vapor Products

Liang Chang, Shuanggen Jin, and Xiufeng He

Abstract—Water vapor variations affect the interferometric synthetic aperture radar (InSAR) signal transmission and the accuracy of the InSAR measurements. The Moderate Resolution Imaging Spectroradiometer (MODIS) near infrared (nIR) water vapor product can correct InSAR atmospheric effects effectively, but it only works for the synthetic aperture radar (SAR) images acquired during the daytime. Although the MODIS infrared (IR) water vapor product owns poorer accuracy and spatial resolution than the nIR product, it is available for daytime as well as nighttime. In order to improve the accuracy of water vapor measurements from the MODIS IR product, a differential linear calibration model (DLCM) has been developed in this paper. The calibrated water vapor measurements from the IR product are then used for wet delay map production and nighttime overpass SAR interferogram atmospheric correction. Results show that the accuracy of the MODIS IR product can be improved effectively after calibration with the DLCM, and the derived wet delays are more suitable for InSAR atmospheric correction than original measurements from the IR product. Furthermore, a MODIS altitude-correlated turbulence model (MATM) is incorporated to correct the atmospheric effects from another descending ASAR interferogram. Results show that the MATM can reduce altitude-dependent water vapor artifacts more effectively than the traditional correction method without the need to incorporate the altitude information.

Index Terms—Atmospheric correction, infrared (IR), interferometric synthetic aperture radar (InSAR), Moderate Resolution Imaging Spectroradiometer (MODIS).

Manuscript received May 28, 2013; revised September 14, 2013; accepted November 10, 2013. This work was supported in part by the Innovation Program of Shanghai Municipal Education Commission under Grant 14YZ118, by the Science Foundation for Doctors of Shanghai Ocean University under Grant A-0209-13-0105395, by the Scientific Research Foundation for National Administration of Surveying, Mapping and Geoinformation Key Laboratory of Land Environment and Disaster Monitoring under Grant LEDM2012B04, by the Main Direction Project of Chinese Academy of Sciences under Grant KJCX2-EW-T03, and by the European Space Agency Category-1 Project under Grant C1P.10660.

L. Chang is with the College of Marine Sciences, Shanghai Ocean University, Shanghai 201306, China, with the National Engineering Research Center for Oceanic Fisheries, Shanghai 201306, China, with the Key Laboratory of Sustainable Exploitation of Oceanic Fisheries Resources, Shanghai Ocean University, Ministry of Education, Shanghai 201306, China, with Collaborative Innovation Center for Distant-water Fisheries, Shanghai 201306, China, and also with the Key Laboratory for Land Environment and Disaster Monitoring of State Bureau of Surveying and Mapping, China University of Mining and Technology, Xuzhou 221116, China (e-mail: chlhwinds@hotmail.com).

S. Jin is with Shanghai Astronomical Observatory, Chinese Academy of Sciences, Shanghai 200030, China (e-mail: sgjin@shao.ac.cn).

X. He is with School of Earth Sciences and Engineering, Hohai University, Nanjing 210098, China (e-mail: xfhe@hhu.edu.cn).

Color versions of one or more of the figures in this paper are available online at <http://ieeexplore.ieee.org>.

Digital Object Identifier 10.1109/TGRS.2013.2292070

I. INTRODUCTION

INTERFEROMETRIC synthetic aperture radar (InSAR) is a very powerful remote sensing technique which has been developed over the past three decades for the measurement of Earth surface topography and deformation [1]. However, one of the limiting noise sources for the repeat-pass InSAR measurements is the atmospheric propagation delay caused by changes in the distribution of atmospheric water vapor, pressure, and temperature [2], [3]. It was reported that a 20% spatial or temporal change of atmospheric relative humidity could result in a deformation measurement error of 10–14 cm or a topographic height error of 80–290 m for perpendicular baselines ranging from 400 to 100 m [4]. As such, the variation in the amount of atmospheric water vapor and other noises between SAR acquisition times is usually hard to distinguish from real ground motion [5].

A number of InSAR atmospheric distortion mitigation methods have been well demonstrated, including using Global Positioning System (GPS) observations (e.g., [6]–[12]), European Centre for Medium-Range Weather Forecasts data (e.g., [13]), nonhydrostatic 3-D (NH3D) models (e.g., [14] and [15]), weather research and forecasting model (e.g., [16] and [17]), and spaceborne optical observations such as the Moderate Resolution Imaging Spectroradiometer (MODIS) (e.g., [18] and [19]) and the Medium Resolution Imaging Spectrometer (MERIS) (e.g., [20]–[23]). The correction method using spaceborne optical observations is, however, different from other methods since their near infrared (nIR) water vapor products can only be available in the daytime. Unlike MERIS, which can monitor precipitable water vapor (PWV) at the nIR band in the daytime only, MODIS can detect the water vapor content using nIR and infrared (IR) bands during both the daytime and nighttime. Although the MODIS IR water vapor product has the advantage in temporal resolution, seldom can it be used for InSAR atmospheric effect correction due to its lower spatial resolution (5 km × 5 km) and poorer accuracy comparing with the nIR product. The former is the secondary reason since the water vapor pixels acquired at the IR band are denser than that of GPS network, which makes it still attractive for correcting atmospheric effects on InSAR, while the latter is the main limitation to mitigate the InSAR atmospheric distortions with MODIS IR water vapor measurements. Thus, if the MODIS IR retrievals can be well calibrated by some model, it will be very promising for correcting atmospheric effects in SAR interferograms at nighttime.

In this paper, we present a differential linear calibration model (DLCM) to calibrate the MODIS IR water vapor product-derived wet delays, and then, the calibrated measurements are used to correct the atmospheric delays on InSAR interferograms over Los Angeles area. The performance of the DLCM will be evaluated and the accuracy of the correction will be assessed with the GPS data of the Southern California Integrated GPS Network (SCIGN). In addition, a MODIS altitude-correlated turbulence model (MATM) built based on the calibrated MODIS nIR water vapor product is incorporated to correct the atmospheric effects of the advanced SAR (ASAR) interferogram in the daytime. The rest of this paper is organized as follows. In Section II, the MODIS water vapor data are introduced, and the accuracy of retrievals at both the nIR and the IR band is estimated via comparisons with GPS observations. Section III presents the MODIS nIR and IR water vapor product calibration model and the calibrated nIR product based altitude-correlated turbulence model. The accuracy evaluation of wet delay from the model output, the applications of the productions of DLCM and MATM to InSAR atmospheric corrections, and their performance assessments are demonstrated in Section IV. Finally, conclusions are addressed in Section V.

II. MODIS NIR AND IR WATER VAPOR PRODUCT DESCRIPTIONS AND ACCURACY ANALYSES

A. MODIS nIR Water Vapor Data

MODIS is equipped onboard the National Aeronautics and Space Administration (NASA) Earth Observing System Terra (launched in December 1999) and Aqua (launched in May 2002) platforms. It detects electromagnetic radiation in 36 visible, nIR, and IR spectral bands between 0.645 and 14.235 μm with spatial resolutions of 250 (2 bands), 500 (5 bands), and 1000 m (29 bands) [24]. Both the Terra and Aqua satellites are in polar sun-synchronous orbit at an altitude of 705 km, and the swath width of the MODIS data for them is 2300 and 2330 km, respectively.

The retrieved nIR MODIS PWV, which is available during the daytime only at a 1 km \times 1 km (at nadir) spatial resolution, is derived from two nonabsorption channels centered near 0.905 and 0.94 μm and three absorption channels centered near 0.865, 0.936, and 1.24 μm [25]. The quality of MODIS nIR retrievals relies on observations of the water vapor attenuation of nIR solar radiation. Therefore, the measurements of MODIS nIR PWV strongly depend on the estimation of surface reflection, which results in that the nIR PWV can only be detected in the daytime only. The MODIS nIR water vapor product-derived PWV is claimed to be determined with an accuracy of 5%–10% [25], and larger error can be introduced over regions where surface reflection is small in nIR channels (e.g., the ocean [26]).

Considering that the MODIS nIR water vapor product may overestimate water vapor compared to the GPS- and the radiosonde-derived PWV, the MODIS nIR PWV needs to be calibrated before its applications [18]. In this paper, we construct the calibration model by linear least squares analysis between MODIS nIR PWV and the continuous GPS observations over SCIGN. Moreover, as MODIS nIR PWV measurements are sensitive to the presence of cloud in the field of view, the

Level 2 MOD05 cloud mask products (collection 5.1) are used to remove the cloudy pixels, and only pixels that showed at least 95% probability of being clear are retained. It should also be noted that the geolocation fields in the MOD05 product only have a 5 km \times 5 km spatial resolution, and the MOD03 geolocation data set needs to be incorporated to obtain the geodetic coordinates for each MODIS nIR 1-km sample.

B. MODIS IR Water Vapor Data

The operational MODIS IR algorithm, which is implemented by a statistical regression algorithm together with an option of a subsequent nonlinear physical retrieval, is used for retrieving vertical temperature and moisture profiles, ozone profiles, precipitable water vapor, and several atmospheric stability indices [27]. The MODIS IR water vapor retrievals are derived from bands 24 to 36 (between 4.47 and 14.24 μm), excluding band 26, and performed using clear sky radiances measured within a 5 \times 5 field of view (approximately 5-km resolution) over land and ocean for both day and night. The PWV at the IR band is generated as one component of product MOD07 and simply added to product MOD05 for convenience.

One of the most prominent disadvantages for the MODIS IR water vapor product is its lower accuracy. MODIS IR PWV over land appears to overestimate (underestimate) in a dry (moist) atmosphere, with the maximum deviation of up to 5 mm and an root mean square error of 4.1–5.2 mm [27], [28]. Therefore, similar with MODIS nIR PWV, the IR PWV also should be calibrated. However, unlike MODIS nIR PWV, few studies devote to enhancing the accuracy of MODIS PWV at the IR band, which may be complementary information for the distribution of changes in water vapor since the MODIS nIR PWV is only available during the daytime while the MODIS IR PWV can be obtained during both the daytime and nighttime. In this paper, we will assess the applicability of traditional linear least squares analysis to calibrate the MODIS IR PWV and analyze the accuracy of PWV measurements before and after calibration.

C. Accuracy Analyses

GPS is able to estimate the PWV with high temporal resolution and high precision, which could be regarded as an ideal tool to analyze the accuracy of MODIS PWV. In this paper, six International Global Navigation Satellite System (GNSS) Service stations over Southern California from January 1, 2008 to May 31, 2009 are adopted (see the black solid squares in Fig. 1) to assess MODIS PWV at both the IR and nIR bands. The contemporaneous MODIS Level 2 water vapor product, the Level 2 cloud mask product, and the Level 1 geolocation products at both nIR and IR bands used to make the comparisons are downloaded from NASA's Goddard Earth Sciences Distributed Active Archive Center (<http://daac.gsfc.nasa.gov>).

Fig. 2 shows the comparison between MODIS nIR PWV under cloud-free conditions and GPS PWV from six GPS observations over SCIGN [see Fig. 2(a)], as well as the scatterplot of MODIS IR PWV in the nighttime and GPS PWV [see Fig. 2(b)]. The differences between MODIS and GPS PWV of greater than two times the standard deviation (STD) were

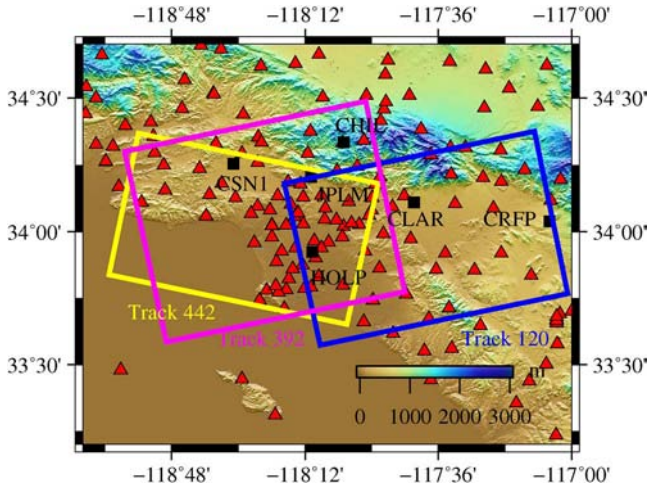


Fig. 1. Distribution of the GPS stations around the ROI with 1-arc sec SRTM shaded relief. The yellow, purple, and blue boxes represent Tracks 442, 392, and 120 of the ENVISAT ASAR interferometric pairs, respectively. Red solid triangles show GPS stations collocated without meteorological sensors, and black solid squares are GPS stations with meteorological sensors.

TABLE I
STD AND THE RMS FOR THE DIFFERENCES OF MODIS PWV FROM GPS PWV (UNIT: MILLIMETER)

Band	Sample number	Errors	Original PWV	Calibrated PWV
nIR	1431	STD	1.247	1.121
		RMS	2.058	1.120
IR (night)	1597	STD	3.658	3.251
		RMS	4.065	3.249

GPS is as high as 0.99, together with the STD and root mean square (rms) of the difference of about 1.25 and 2.06 mm, respectively. However, the performance of MODIS IR PWV in the nighttime is quite poor, which is shown in Fig. 2(b). The STD and rms of the difference between MODIS IR and GPS PWV were 3.66 and 4.07 mm, respectively. The inferior performance of the IR retrievals implies that the uncertainty associated with MODIS IR PWV is greater than that associated with MODIS nIR PWV.

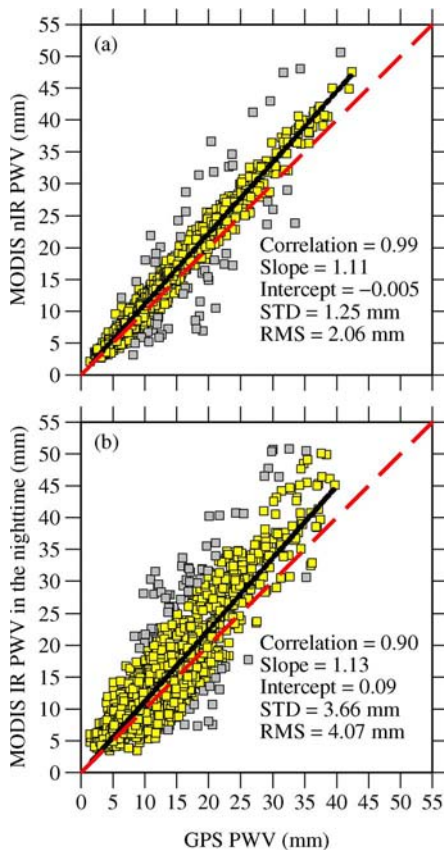


Fig. 2. Scatterplots between MODIS PWV under cloud-free condition and GPS PWV: (a) MODIS nIR in the daytime and GPS PWV and (b) MODIS IR PWV in the nighttime and GPS PWV. Note that the gray solid squares are considered as outliers and are removed due to the 2σ exclusion.

regarded as outliers and were not incorporated to build the calibration model via linear least squares analysis. It can be seen from Fig. 2(a) that the MODIS nIR PWV agrees very well with GPS PWV, particularly in drier atmosphere. In addition, the variation of the differences became larger as the PWV increased. The correlation coefficient between MODIS nIR and

III. MODIS WATER VAPOR PRODUCT CALIBRATION MODEL AND ALTITUDE-CORRELATED TURBULENCE MODEL

A. Traditional Linear Least Square Calibration Model

Based on the linear least square analysis of MODIS nIR PWV with respect to GPS PWV, a calibrated model is yielded as follows:

$$\text{cali_PWV}_{\text{nIR}} = 0.90 \times \text{PWV}_{\text{nIR}} + 0.004. \quad (1)$$

Similar with nIR retrievals, a linear relationship between MODIS IR PWV in the nighttime and GPS PWV is also obtained as

$$\text{cali_PWV}_{\text{IR}} = 0.89 \times \text{PWV}_{\text{IR}} + 0.08. \quad (2)$$

In order to assess the capability of the derived model by linear regression analysis, comparisons of differences of nIR and IR retrievals from GPS PWV were made, which are shown in Table I. It can be seen from Table I that, after calibration, the STD and rms of the difference for nIR retrievals decreased from 1.25 to 1.12 mm and 2.06 to 1.12 mm, respectively, indicating an improvement of 10.1% and 45.6%. For IR retrievals in the nighttime, the STD difference reduced from 3.66 to 3.26 mm with an improvement of 10.9%, and the rms difference falls from 4.07 to 3.25 mm with an improvement of 20.2%. Taking into account the large STD (i.e., > 3 mm) of the linear fit model for IR retrievals in the nighttime both before and after calibration, the traditional linear least square model [i.e., (2)] may not be an optimal choice to calibrate MODIS IR PWV in the nighttime.

B. MATM

The atmospheric delay can be distinguished as two parts [29]: 1) atmospheric turbulent processes resulting in turbulent mixing, which similarly affects plains and mountains, and 2) vertical stratification caused by different vertical refractivity

profiles during the two SAR acquisitions, which is correlated with topography. In this paper, the Onn water vapor model is adopted to estimate the vertical stratification part of the atmospheric signal by [11]

$$D_{\text{Onn}} = Ce^{-\alpha h} + h\alpha Ce^{-\alpha h} + d_{\text{min}} \quad (3)$$

where d_{min} is the wet delay recorded at the highest altitude station, h represents the altitude of the wet delay value, C is proportional to the amount of wet delay measured at sea level, and α is the delay rate of the vertical water vapor profile.

In order to evaluate the uncertainty of the Onn model effectively, the goodness of fit of the modeled zenith wet delay (ZWD) to the MODIS nIR wet delay in terms of chi-square statistic was estimated by [11]

$$\chi_n^2 = \frac{1}{n-2} \sum_{i=1}^n \frac{(\text{ZWD}_{\text{MODIS}}(p_i) - \text{ZWD}_{\text{Onn}}(p_i))^2}{\sigma_{\text{GPS}}^2} \quad (4)$$

where n is the number of MODIS water vapor pixels used for the Onn model construction, $n-2$ denotes the degrees of freedom of the chi-square statistic, $\text{ZWD}_{\text{MODIS}}(p_i)$ corresponds to wet delays obtained from the MODIS water vapor product at pixel p_i , $\text{ZWD}_{\text{Onn}}(p_i)$ represents the Onn modeled wet delay $\text{ZWD}_{\text{MODIS}}(p_i)$, and σ_{GPS} is the GPS ZWD estimation error of 4 mm.

In this paper, unlike Li *et al.* [22] who constructed the wet delay map using MERIS data by the simple-kriging-with-varying-local-means estimator and Onn model, we focus on estimating the altitude-correlated wet delay map via a MATM by

$$D(p) = \sum_{i=1}^n w_i (D_{\text{MODIS}}(p_i) - D_{\text{Onn}}(p_i)) + D_{\text{Onn}}(p) \quad (5)$$

where $D(p)$ is the wet delay derived at pixel p by MATM, n is the number of MODIS water vapor pixels, w_i denotes the weight of inverse distance weight (IDW) interpolation, $D_{\text{MODIS}}(p_i)$ represents the wet delay detected by the MODIS water vapor product at pixel p_i , and $D_{\text{Onn}}(p_i)$ and $D_{\text{Onn}}(p)$ can be estimated using the Onn model [viz., (3)]. After the wet delay distribution is generated with the MATM, it can then be used for InSAR atmospheric effect correction.

C. DLCM for MODIS IR PWV

In order to calibrate the MODIS IR retrievals more effectively, a DLCM is developed and can be performed as follows (see Fig. 3).

- 1) Obtain the reference PWV values from reliable tools (e.g., GPS and radiosonde and microwave radiometer observations), and estimate the PWV values at the MODIS image pass time by temporal interpolation (e.g., spline interpolation).
- 2) Extract PWV values from the MODIS IR water vapor product at colocations of reference PWV measurements in (1) by spatial interpolation (e.g., IDW interpolation).
- 3) Subtract reference PWV (designated as PWV_{ref}) from MODIS IR PWV (designated as PWV_{IR}), and get their differential component, which can be defined as $\text{delta1} = \text{PWV}_{\text{IR}} - \text{PWV}_{\text{ref}}$. Implement the traditional linear least

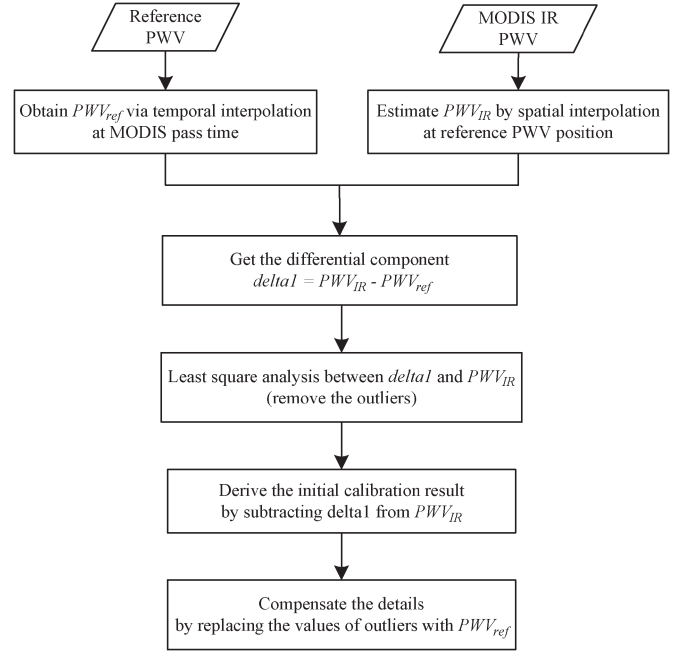


Fig. 3. Flowchart of DLCM.

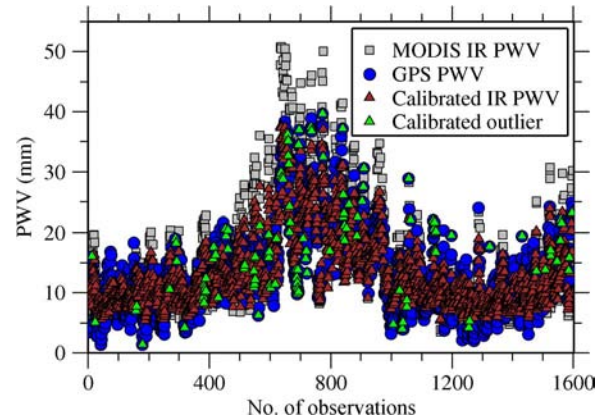


Fig. 4. Calibration of MODIS IR PWV over Southern California from January 1, 2008 to May 31, 2009 with DLCM. Gray solid squares represent the original MODIS IR retrievals, blue solid circles are the reference PWV derived from GPS observations, brown solid triangles denote the IR retrievals calibrated by DLCM, and green solid triangles are calibration for outliers.

square analysis between delta1 and PWV_{IR} to derive their relationship. Note that the difference between delta1 and PWV_{IR} exceeding twice the STD should also be removed.

- 4) Subtract again delta1 from PWV_{IR} , and the difference is recognized as the initial calibration result.
- 5) Some reference PWV measurements that have pretty large deviation may be recognized as outliers and be omitted during the calibration. In order to avoid losing the details when detecting the moisture information with MODIS IR retrievals, we compensate the information by replacing the values of outliers with the reference PWV measurements.

After calibration with the developed DLCM, the overestimated MODIS IR PWV measurements are relieved, from which we gain closer moisture information to GPS PWV than that from original IR retrievals (shown in Fig. 4). The rms difference

TABLE II
DESCRIPTIONS OF INTERFEROGRAMS (Ifms) USED IN THIS STUDY

	Master	Delta time (minutes)	Slave	Delta time (minutes)	Track	Frame	Time span (days)	B ₁ (m)
Ifm 1	13-Mar-2008	31	07-May-2009	11	442	2925	420	53 to 59
Ifm 2	04-Feb-2008	-7	14-Apr-2008	53	392	675	35	160 to 167
Ifm 3	11-Mar-2009	35	18-Aug-2010	5	120	675	525	14 to 30

between GPS and MODIS IR PWV decreases to 2.83 mm after calibration using DLCM, which implies that it gains an extra 10.2% improvement comparing to the calibration with the traditional linear fit model. Moreover, after the lost details are compensated, the STD and rms difference further reduce to 2.14 and 2.44 mm, respectively, indicating that the new calibration model is promising.

IV. CASE STUDY OF INSAR ATMOSPHERIC EFFECT CORRECTION BASED ON MODIS WATER VAPOR PRODUCTS

A. Study Area and Data Processing Strategy

The Southern California, USA, is selected as the region of interest (ROI) to test the performance of MODIS-derived wet delay on InSAR atmospheric effect correction, due to the high frequency of cloud-free conditions, as well as one of the densest regional GPS networks in this area [18]. In this paper, three pairs of the European Space Agency's ENVISAT ASAR data over the Los Angeles region are used for experiments. One of them was acquired from a descending pass in the daytime, while the others were acquired at nighttime from ascending passes (see Fig. 1 and Table II). Note that the delta time in Table II means the time difference between SAR and MODIS acquisitions, and the positive values indicate that the MODIS overpass time was later than that of the SAR images. In this paper, the time differences of less than 1 h were neglected during InSAR correction due to previous successful experiences [18].

The SAR interferometric pairs were processed with GAMMA Remote Sensing software by the two-pass Differential InSAR approach. Precise orbit state vectors provided by the Doppler Orbitography and Radio-positioning Integrated by Satellite instrument were employed to assist SAR image coregistration, reduce baseline errors, and remove the flat Earth phase. The 1-arc sec (~ 30 m) digital elevation model (DEM) from the Shuttle Radar Topography Mission (SRTM) [30] was employed to simulate the height map in the SAR coordinate system and remove the topographic phase contribution in interferograms. To suppress the noise in the interferograms, the SAR pairs were implemented with multilook processing of 40 pixels in the azimuth and 8 pixels in the range directions, which derives a final resolution of about 160 m by 160 m. The interferograms were then smoothed by adaptive filtering followed with phase unwrapping by the branch-cut method [31] with the coherence threshold set to be 0.5. The baselines were refined next using the unwrapped phase and the independent DEM, which can help to generate more reasonable values for area with low coherence. Moreover, a 2-D quadratic model phase function from the differential interferogram was

also estimated to mitigate possible orbital errors. At last, the unwrapped interferograms were mapped into the line of sight (LOS) direction in the universal transverse mercator coordinate system, and the unwrapped phase values were converted to deformation distances.

In this paper, the MODIS nIR and IR water vapor products were adopted to correct the descending pass SAR pairs (i.e., Ifm 1) at daytime and ascending pass SAR pairs (i.e., Ifms 2 and 3) at nighttime, respectively. Considering the relative worse accuracy of the IR product than the nIR one, the former was calibrated with developed DLCM, while the latter was processed with (1). Furthermore, taking into account the high relationship between wet delay and topography, the MATM was incorporated to construct the wet delay map, including both turbulent mixing and vertical stratification.

In order to evaluate the performance of the correction methods objectively, the precise 3-D surface displacements from each GPS site at SAR pass time, which can be obtained from the Scripps Epoch Coordinate Tool and Online Resource [32], were differentiated and projected to the radar LOS direction for comparisons with InSAR measurements

$$d_{LOS} = [\sin \theta \sin \alpha_h \quad -\sin \theta \cos \alpha_h \quad \cos \theta] \begin{bmatrix} U_n \\ U_e \\ U_u \end{bmatrix} \quad (6)$$

where d_{LOS} denotes the LOS displacement, α_h is the azimuth of the satellite heading vector (positive clockwise from the north), θ is the radar incidence angle at the reflection point, and U_n , U_e , and U_u are the northing, easting, and vertical displacement vectors, respectively.

B. Atmospheric Correction

1) *Descending Interferogram—March 13, 2008–May 7, 2009*: Fig. 5 shows the Onn water vapor model resulting fits to the MODIS nIR wet delays, as well as the inferred regression parameters for the master and slave SAR images of interferogram March 13, 2008–May 7, 2009 (i.e., Ifm 1). As illustrated in Fig. 5, the MODIS nIR retrievals match quite well with the Onn model outputs except that unideal deviations exist in moisture atmosphere (viz., at low altitudes). Moreover, the performance of the fit to nIR ZWD at the slave SAR overpass time was slightly poorer than that at the master SAR acquisition time, and the chi-square statistics of the fits were 3.51 mm for the former and 2.16 mm for the latter.

The Onn modeled wet delays were used to estimate the ZWD maps which can then be converted into the SAR LOS direction using the simplest mapping function $1/\cos \theta$, where θ is the incidence angle of each SAR image pixel. Fig. 6 shows the

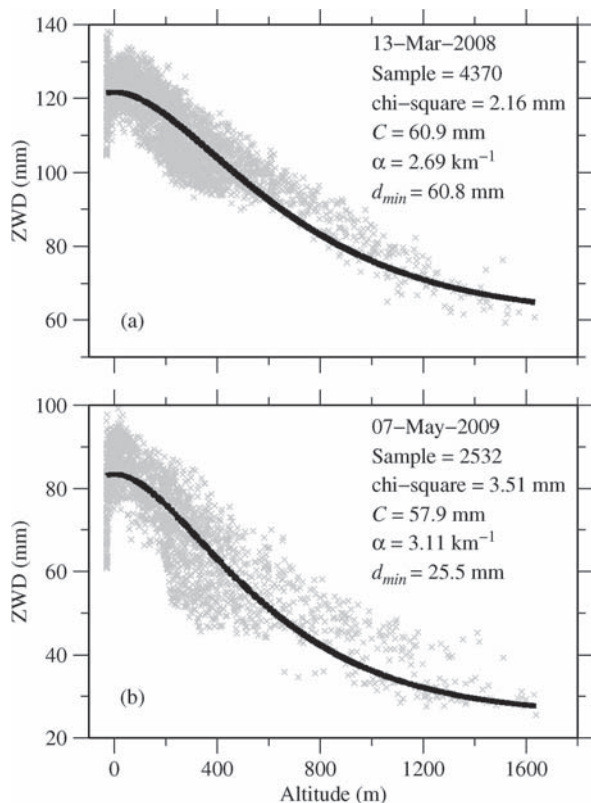


Fig. 5. (Gray cross) Least squares regressions between MODIS nIR-derived ZWDs and MODIS pixel altitudes at the SAR overpass times on (a) Mar 13, 2008 and (b) May 7, 2009. The black lines correspond to the least squares fits to the nIR ZWD data at the two SAR overpass times.

original unwrapped phase [see Fig. 6(a)], the corrected phase by the MODIS nIR water vapor product [see Fig. 6(b)], the corrected phase by MATM [see Fig. 6(c)], and the difference between Fig. 6(b) and (c) for Ifm 1, respectively. It is clear from Fig. 6 that the negative (northwest corner) and positive (upper middle part) surface displacement signals of the original Ifm 1 were reduced to a large extent after correction, implying that the MODIS nIR retrievals can be used for InSAR atmospheric delay corrections effectively. In order to evaluate the capability of MATM, the difference of the corrected phase by MATM from that by MODIS nIR water vapor retrievals was given in Fig. 6(d). As can be seen in Fig. 6(d), the differences of the unwrapped phases in Fig. 6(b) and (c) exist primarily in areas of high relief, and the negative signal in the bottom of Fig. 6(d) (marked by black rectangle) indicated that Fig. 6(c) gains more improvement on relieving InSAR atmospheric effects than Fig. 6(b). Therefore, it can be further deduced that the MATM works more efficiently than the MODIS IDW method. The phase variations in terms of STD of Ifm 1 decreased from 7.53 mm without correction [see Fig. 6(a)] to 6.41 mm after mitigating with MODIS nIR water vapor retrievals but without incorporating the altitude information [see Fig. 6(b)]. Furthermore, when the MATM was used, the phase variation further reduced to 6.27 mm [see Fig. 6(c)].

In Fig. 7, comparisons of ground displacements detected by GPS and InSAR in the SAR LOS direction, together with the altitudes of GPS sites, are shown. It was found in Fig. 7 that the LOS displacements estimated by InSAR measurements

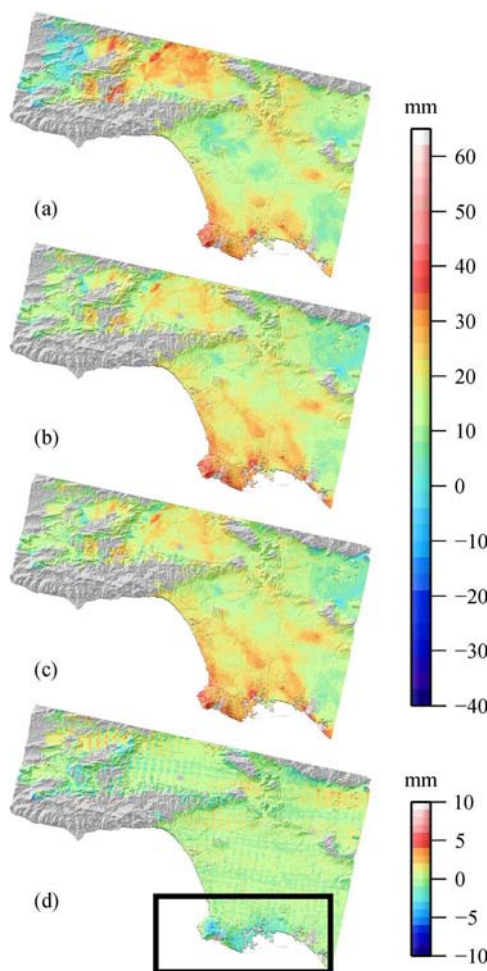


Fig. 6. Unwrapped phases for Ifm 1 overlaid on SRTM DEM shaded relief map. (a) Original. (b) Corrected with MODIS IDW method. (c) Corrected by MATM. (d) (c)–(b). Note that negative values denote that the ground surface moves away from the satellite (i.e., subsidence).

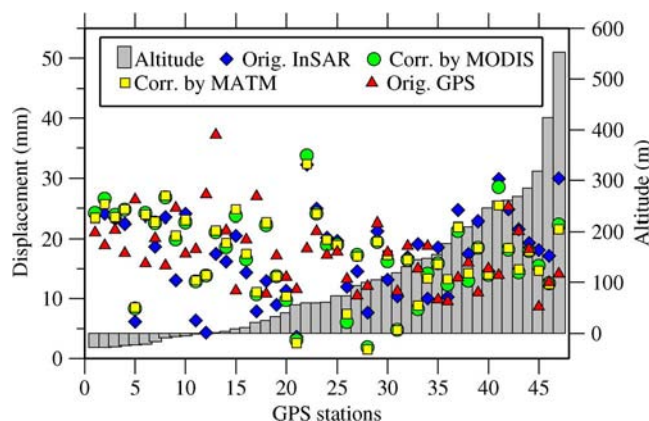


Fig. 7. Comparisons of LOS displacements detected by InSAR and GPS measurements (Ifm 1).

appear closer to the information of GPS detections at most sites after correction. Moreover, the MATM can achieve more improvements at both areas of high relief and flat terrain. After correction with the MODIS IDW method, the rms differences between the InSAR and GPS measurements reduced from 9.4 to 8.0 mm, while that further dropped to 7.6 mm after applying the MATM.

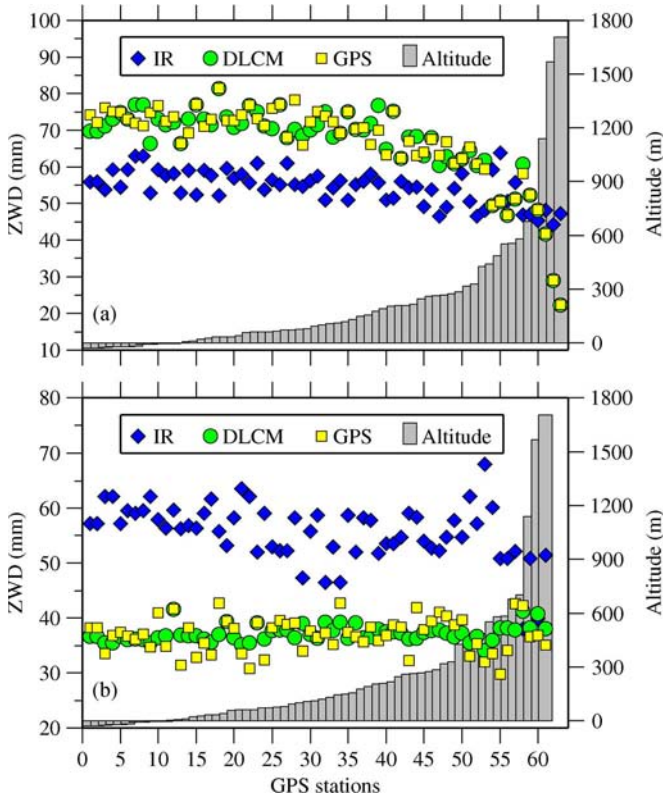


Fig. 8. Calibration of MODIS IR ZWD with DLCM for Ifm 2. (a) February 4, 2008. (b) April 14, 2008.

2) *Ascending Interferogram—February 4, 2008–April 14, 2008*: The SAR satellites are capable of monitoring the Earth’s surface at the nighttime, when only MODIS PWV measurements at the IR band are available. Fig. 8 shows the comparisons among the MODIS IR ZWD, calibrated IR ZWD by DLCM, and ZWD from GPS measurements for interferogram February 4, 2008–April 14, 2008 (i.e., Ifm 2). As can be seen in Fig. 8, large differences can be observed between the original IR ZWD and GPS ZWD, while the calibrated ZWD measurements by DLCM match the GPS ZWD quite well. The rms differences between IR ZWD and GPS ZWD were 15.7 and 19.9 mm at the master and the slave image overpass time, while that reduced to 2.9 and 2.8 mm after calibration with DLCM, respectively. However, the calibrated IR ZWD measurements were not adopted for further generating the wet delay map with MATM because they did not exhibit an obvious exponential decay law as altitudes increase [see Fig. 8(b)].

Fig. 9 shows the original interferometric phase and the corrected results for Ifm 2. We can see in Fig. 9(a) that the atmospheric signals of Ifm 2 were poorly correlated with the topography of the study area. The phase variation in terms of STD of the unwrapped phase for the original Ifm 2 [see Fig. 9(a)] was 12.3 mm. After correction with GPS-derived wet delay, the STD of Ifm 2 decreased to 11.3 mm [see Fig. 9(b)], while the STD reduced to 11.5 and 11.6 mm with the MODIS IR ZWD [see Fig. 9(c)] and the DLCM ZWD [see Fig. 9(d)] correction, respectively. Comparisons of GPS- and InSAR-derived ground displacements in the SAR LOS direction were illustrated in Fig. 10. It can be observed in Fig. 10 that large differences between the InSAR- and GPS-detected displacements primarily

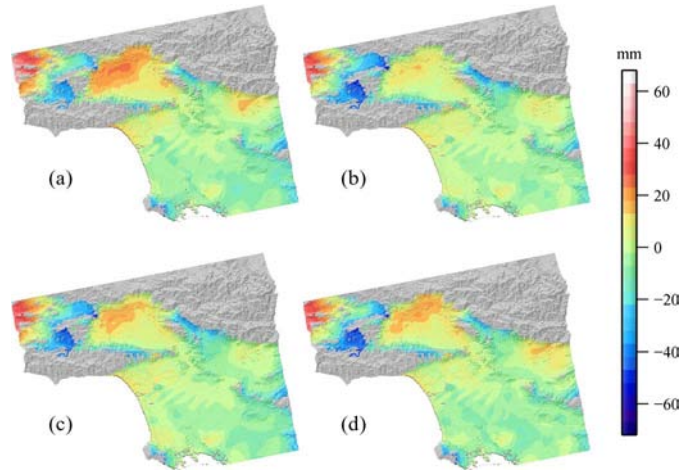


Fig. 9. Unwrapped phases for Ifm 2 overlaid on SRTM DEM shaded relief map. (a) Original. (b) Corrected with GPS observations. (c) Corrected with MODIS IR ZWD directly. (d) Corrected with DLCM ZWD. Note that negative values denote that the ground surface moves away from the satellite (i.e., subsidence).

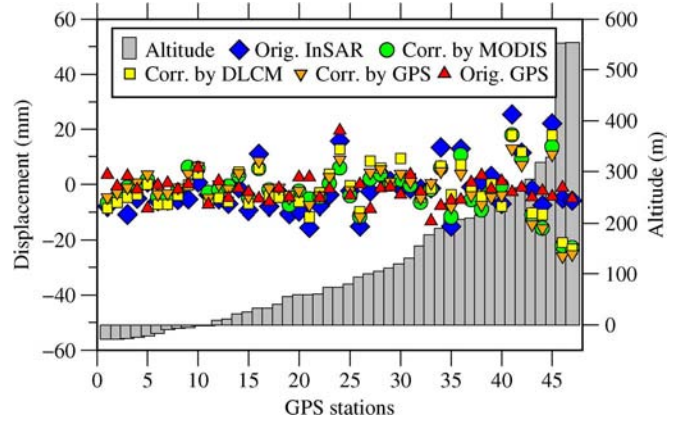


Fig. 10. Comparisons of LOS displacements detected by InSAR and GPS measurements (Ifm 2).

occurred at higher altitudes, and the deviations were shrunk after correction. Moreover, after correction with GPS observations, the InSAR-derived displacements gained better results than the other measurements shown in Fig. 10, implying that the GPS observations can help to reduce InSAR water vapor signals much better than MODIS IR retrievals. Quantitative results showed that the rms differences between GPS and corrected InSAR measurements by GPS decreased from 10.0 to 8.9 mm, while that dropped to 9.0 and 9.5 mm after correction with MODIS IR ZWD and DLCM ZWD, respectively.

As mentioned in Sections II and III, the MODIS IR ZWD needs to be calibrated due to its low accuracy. However, comparisons shown in Figs. 9 and 10 revealed that the MODIS IR ZWD can also help to mitigate the atmospheric distortions to some extent. One possible reason might be that the uncertainty of the MODIS moisture information was caused by systematic errors, which could be removed or reduced by differentiating between SAR interferometric pairs. In order to check whether the errors of MODIS IR ZWD can be removed by the differentiating process or not, another ascending case (i.e., Ifm 3) was chosen for further analysis.

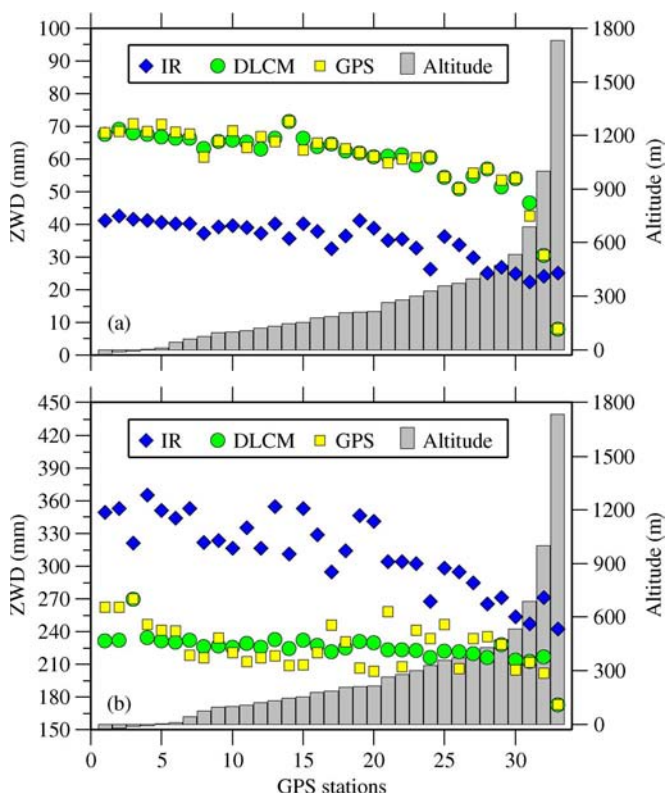


Fig. 11. Calibration of MODIS IR ZWD with DLCM for Ifm 3. (a) March 11, 2009. (b) August 18, 2010.

3) *Ascending Interferogram—March 11, 2009–August 18, 2010*: ZWD measurements from the original MODIS IR water vapor product, DLCM, and GPS observations were given in Fig. 11 for interferogram March 11, 2009–August 18, 2010 (i.e., Ifm 3). The rms differences between IR ZWD and GPS ZWD were 25.8 and 92.7 mm at the master and the slave image overpass time, while that reduced to 3.3 and 19.6 mm after calibration with DLCM, respectively. The improvements of about 87.2% in a dry atmosphere [see Fig. 11(a)] and 78.9% in a moist atmosphere [see Fig. 11(b)] have been achieved, indicating that the DLCM will not be affected by atmospheric humidity.

In Fig. 12, we can see that the unwrapped phases have been removed effectively after correction with GPS observations [see Fig. 12(b)] and relieved with the help of calibrated IR ZWD by DLCM [see Fig. 12(d)]. However, the residual phases got worse during correction with the MODIS IR ZWD directly [see Fig. 12(c)]. Comparing to the phase variations of the unwrapped phase that decreased from the original 13.6 mm [see Fig. 12(a)] to 12.5 mm in Fig. 12(b), as well as that which reduced to 13.3 mm in Fig. 12(d), the STD increased to 33.1 mm after MODIS IR ZWD correction [see Fig. 12(c)]. Furthermore, comparisons of GPS- and InSAR-detected LOS ground displacements of Ifm 3 shown in Fig. 13 also illustrated the incapability of correcting InSAR atmospheric distortion with MODIS IR ZWD directly. After applying correction with GPS observations and DLCM ZWD, the rms differences between GPS and InSAR displacements decreased from 18.3 to 13.3 and 17.8 mm, respectively, while the rms increased to 33.3 mm after correction with MODIS IR ZWD directly. Therefore, after

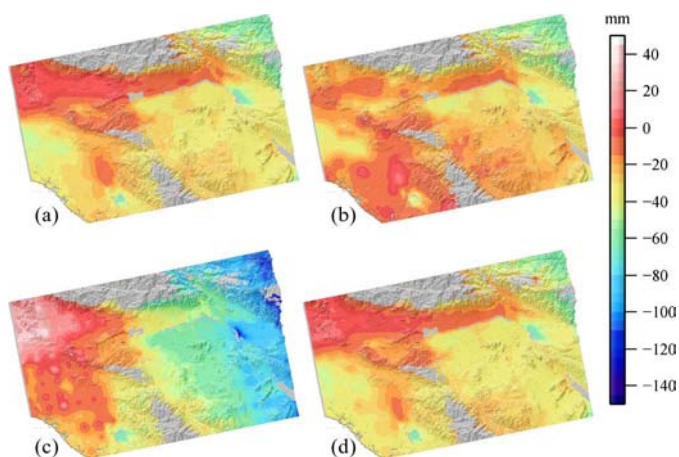


Fig. 12. Unwrapped phases for Ifm 3 overlaid on SRTM DEM shaded relief map. (a) Original. (b) Corrected with GPS observations. (c) Corrected with MODIS IR ZWD directly. (d) Corrected with DLCM ZWD. Note that negative values denote that the ground surface moves away from the satellite (i.e., subsidence).

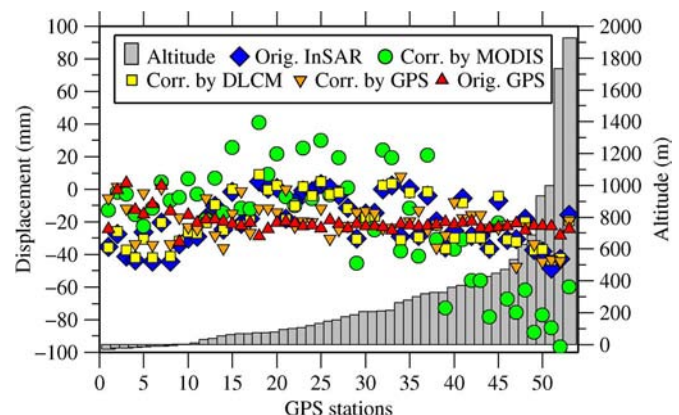


Fig. 13. Comparisons of LOS displacements detected by InSAR and GPS measurements (Ifm 3).

correction with MODIS IR ZWD directly, the atmospheric artifacts for Ifm 2 may be reduced by coincidence. It can also be concluded that the MODIS IR ZWD should be calibrated appropriately before it was used for InSAR atmospheric effect correction, and the calibrated IR ZWD was helpful to relieve the InSAR atmospheric noise.

V. CONCLUSION

In this paper, we assess the performance of MODIS nIR and IR water vapor products on InSAR atmospheric correction. In order to correct the atmospheric artifacts in repeat-pass interferometry during the daytime with the MODIS nIR water vapor product, a MATM is incorporated to generate the altitude-correlated atmospheric delay. Moreover, a DLCM has been developed for the atmospheric distortion mitigation of interferometric SAR pairs during the nighttime. Our findings from this study can be summarized as follows.

- 1) The accuracies of MODIS nIR and IR PWVs can both be enhanced after calibration via linear regression analysis, with an rms improvement of 45.6% for nIR retrievals and 20.2% for IR retrievals, respectively. In addition, after the DLCM was applied to IR retrievals, an extra 19.9%

improvement has been achieved, indicating that the calibration of MODIS IR PWV with DLCM is promising.

- 2) After the altitude information was incorporated for InSAR atmospheric correction, the MATM with nIR retrievals worked more efficiently than the MODIS IDW method. The application of MATM to interferometric SAR pairs at daytime showed that not only could it reduce the altitude-dependent residual phases, but also, it helped to mitigate the distortions in flat terrain.
- 3) The MODIS IR-derived wet delays needed to be calibrated properly before they were used for InSAR atmospheric effect correction. Furthermore, the uncertainty of IR retrievals cannot be reduced by differentiation between master and slave images. As such, the effectiveness of the MODIS IR ZWD shown in Ifm 2 can be considered as an unusual coincidence.
- 4) The calibrated MODIS IR ZWD by DLCM can help to relieve the InSAR water vapor artifacts during the nighttime. After correction with DLCM ZWD, the InSAR measurements performed better than the phases corrected by the original IR ZWD.

However, some limitations and challenges remain in using the MODIS water vapor product to mitigate the InSAR atmospheric effects. First, the MODIS water vapor product needs to be properly calibrated before it was used for InSAR atmospheric correction. Second, the MODIS water vapor product only works on cloud-free conditions. Finally, although the accuracy of the MODIS IR water vapor product was improved after being calibrated with DLCM, it can only gain inferior reduction of atmospheric artifacts to the correction with GPS observation. The most possible reason may lie in the large inherent errors for the MODIS IR retrievals. However, it is evident that the developed DLCM can improve the accuracy of IR retrievals greatly, so further improvements may be achieved if a more efficient calibration model can be found, which would be an important issue in future.

ACKNOWLEDGMENT

The authors would like to thank Prof. C. Ruf, Prof. A. Plaza, the associate editor, and three anonymous reviewers for their guiding and constructive comments. The authors would also like to thank Dr. Z. Wu (The Hong Kong Polytechnic University) for his useful discussions.

REFERENCES

- [1] S. M. Buckley, "Radar interferometry measurement of land subsidence," Ph.D. dissertation, Univ. Texas Austin, Austin, TX, USA, 2000.
- [2] R. F. Hanssen, *Atmospheric Heterogeneities in ERS Tandem SAR Interferometry*. Delft, The Netherlands: Delft Univ. Press, 1998, ch. 2, pp. 5–24.
- [3] M. P. Doin, C. Lasserre, G. Peltzer, O. Cavalié, and C. Doubr, "Corrections of stratified tropospheric delays in SAR interferometry: Validation with global atmospheric models," *J. Appl. Geophys.*, vol. 69, no. 1, pp. 35–50, Sep. 2009.
- [4] H. A. Zebker, P. A. Rosen, and S. Hensley, "Atmospheric effects in interferometric synthetic aperture radar surface deformation and topographic maps," *J. Geophys. Res.*, vol. 102, no. B4, pp. 7547–7563, Apr. 1997.
- [5] J. Foster, B. Brooks, T. Cherubini, C. Shacat, S. Businger, and C. L. Werner, "Mitigating atmospheric noise for InSAR using a high resolution weather model," *Geophys. Res. Lett.*, vol. 33, no. 16, pp. L16304–L16304-5, Aug. 2006.
- [6] S. Williams, Y. Bock, and P. Fang, "Integrated satellite interferometry: Tropospheric noise, GPS estimates and implications for interferometric synthetic aperture radar products," *J. Geophys. Res.*, vol. 103, no. B11, pp. 27 051–27 068, Nov. 1998.
- [7] G. Wadge, P. W. Webley, I. N. James, R. Bingley, A. Dodson, S. Waugh, T. Veneboer, G. Puglisi, M. Mattia, D. Baker, S. C. Edwards, S. J. Edwards, and P. J. Clarke, "Atmospheric models, GPS and InSAR measurements of the tropospheric water vapour field over Mount Etna," *Geophys. Res. Lett.*, vol. 29, no. 19, pp. 11.1–11.4, Oct. 2002.
- [8] Z. Li, E. J. Fielding, P. Cross, and J. P. Muller, "Interferometric synthetic aperture radar atmospheric correction: GPS topography-dependent turbulence model," *J. Geophys. Res.*, vol. 111, no. B2, pp. B02404-1–B02404-12, Feb. 2006.
- [9] Z. W. Li, X. L. Ding, C. Huang, and D. W. Zheng, "Modeling of atmospheric effects on InSAR measurements by incorporating terrain elevation information," *J. Atmos. Sol.–Terr. Phys.*, vol. 68, no. 11, pp. 1189–1194, Jul. 2006.
- [10] Z. W. Li, X. L. Ding, W. Chen, G. X. Liu, Y. K. Shea, and N. Emerson, "Comparative study of tropospheric empirical model for Hong Kong region," *Survey Rev.*, vol. 40, no. 31, pp. 328–341, Oct. 2008.
- [11] F. Onn and H. A. Zebker, "Correction for interferometric synthetic aperture radar atmospheric phase artifacts using time series of zenith wet delay observations from a GPS network," *J. Geophys. Res.*, vol. 111, no. B9, p. B09102, Sep. 2006.
- [12] L. Chang and X. He, "InSAR atmospheric distortions mitigation: GPS observations and NCEP FNL data," *J. Atmos. Sol.–Terr. Phys.*, vol. 73, no. 4, pp. 464–471, Mar. 2011.
- [13] R. Jolivet, R. Grandin, C. Lasserre, M.-P. Doin, and G. Peltzer, "Systematic InSAR tropospheric phase delay corrections from global meteorological reanalysis data," *Geophys. Res. Lett.*, vol. 38, no. 17, pp. L17311-1–L17311-6, Sep. 2011.
- [14] P. W. Webley, G. Wadge, and I. N. James, "Determining radio wave delay by non-hydrostatic atmospheric modeling of water vapor over mountains," *Phys. Chem. Earth*, vol. 29, no. 2/3, pp. 139–148, 2004.
- [15] G. Wadge, M. Zhu, R. J. Holley, I. N. James, P. A. Clark, C. Wang, and M. J. Woodage, "Correction of atmospheric delay effects in radar interferometry using a nested mesoscale atmospheric model," *J. Appl. Geophys.*, vol. 72, no. 2, pp. 141–149, Oct. 2010.
- [16] G. Nico, R. Tome, J. Catalao, and P. M. A. Miranda, "On the use of the WRF model to mitigate tropospheric phase delay effects in SAR interferograms," *IEEE Trans. Geosci. Remote Sens.*, vol. 49, no. 12, pp. 4960–4976, Dec. 2011.
- [17] P. Mateus, G. Nico, R. Tome, J. Catalao, and P. M. A. Miranda, "Experimental study on the atmospheric delay based on GPS, SAR interferometry, and numerical weather model data," *IEEE Trans. Geosci. Remote Sens.*, vol. 51, no. 1, pp. 6–11, Jan. 2013.
- [18] Z. Li, J. P. Muller, P. Cross, and E. J. Fielding, "Interferometric synthetic aperture radar (InSAR) atmospheric correction: GPS, Moderate Resolution Imaging Spectroradiometer (MODIS), and InSAR integration," *J. Geophys. Res.*, vol. 110, no. B3, pp. B03410-1–B03410-10, Mar. 2005.
- [19] Z. Li, E. J. Fielding, P. Cross, and R. Preusker, "Advanced InSAR atmospheric correction: MERIS/MODIS combination and stacked water vapour models," *Int. J. Remote Sens.*, vol. 30, no. 13, pp. 3343–3363, Jan. 2009.
- [20] Z. Li, E. J. Fielding, P. Cross, and J. P. Muller, "Interferometric synthetic aperture radar atmospheric correction: Medium Resolution Imaging Spectrometer and Advanced Synthetic Aperture Radar integration," *Geophys. Res. Lett.*, vol. 33, no. 6, pp. L06816-1–L06816-4, Mar. 2006.
- [21] Z. Li, P. Pasquali, A. Cantone, A. Singleton, G. Funning, and D. Forrest, "MERIS atmospheric water vapor correction model for wide swath interferometric synthetic aperture radar," *IEEE Geosci. Remote Sens. Lett.*, vol. 9, no. 2, pp. 257–261, Mar. 2012.
- [22] P. Mateus, G. Nico, and J. Catalao, "Interpolating MERIS and GPS measurements of precipitable water vapour (PWV) to estimate atmospheric phase delay maps," in *Proc. SPIE*, 2010, pp. 782 713-1–782 713-1.
- [23] Z. W. Li, W. B. Xu, G. C. Feng, J. Hu, C. C. Wang, X. L. Ding, and J. J. Zhu, "Correcting atmospheric effects on InSAR with MERIS water vapor data and elevation-dependent interpolation model," *Geophys. J. Int.*, vol. 189, no. 2, pp. 898–910, May 2012.
- [24] M. D. King, Y. J. Kaufman, W. P. Menzel, and D. Tanre, "Remote sensing of cloud, aerosol, and water vapor properties from the Moderate Resolution Imaging Spectrometer (MODIS)," *IEEE Trans. Geosci. Remote Sens.*, vol. 30, no. 1, pp. 2–27, Jan. 1992.
- [25] B. C. Gao and Y. J. Kaufman, "Water vapor retrievals using Moderate Resolution Imaging Spectroradiometer (MODIS) near-infrared channels," *J. Geophys. Res.*, vol. 108, no. D13, pp. 4389–4398, Jul. 2003.

- [26] R. G. Kleidman, Y. J. Kaufman, B. C. Gao, L. A. Remer, V. G. Brackett, R. A. Ferrare, E. V. Browell, and S. Ismail, "Remote sensing of total precipitable water vapor in the near-IR over ocean glint," *Geophys. Res. Lett.*, vol. 27, no. 17, pp. 2657–2660, Sep. 2000.
- [27] S. W. Seemann, J. Li, W. P. Menzel, and L. E. Gumley, "Operational retrieval of atmospheric temperature, moisture, and ozone from MODIS infrared radiances," *J. Appl. Meteorol.*, vol. 42, no. 8, pp. 1072–1091, Aug. 2003.
- [28] S. H. Chen, Z. Zhao, J. S. Haase, A. D. Chen, and F. Vandenberghe, "A study of the characteristics and assimilation of retrieved MODIS total precipitable water data in severe weather simulations," *Mon. Weather Rev.*, vol. 136, no. 8, pp. 3608–3628, Aug. 2008.
- [29] R. F. Hanssen, *Radar Interferometry, Data Interpretation and Error Analysis*. Dordrecht, The Netherlands: Kluwer, 2001.
- [30] T. G. Farr and M. Kobrick, "Shuttle radar topography mission produces a wealth of data," *EOS, Trans. Amer. Geophys. Union*, vol. 81, no. 48, pp. 583–585, Nov. 2000.
- [31] R. M. Goldstein, H. A. Zebker, and C. L. Werner, "Satellite radar interferometry: Two dimensional phase unwrapping," *Radio Sci.*, vol. 23, no. 4, pp. 713–720, Jul./Aug. 1988.
- [32] R. Nikolaides, "Observation of geodetic and seismic deformation with the global positioning system," Ph.D. dissertation, Univ. California, San Diego, CA, USA, 2002.



Shuanggen Jin was born in Anhui, China, in 1974. He received the B.Sc. degree in geodesy/geomatics from Wuhan University, Wuhan, China, in 1999 and the Ph.D. degree in GNSS/geodesy from the University of Chinese Academy of Sciences, Beijing, China, in 2003.

Since 2004, he has been a Visiting Fellow at the University of New South Wales, Sydney, Australia, Post-Doc and Senior Scientist at the Korea Astronomy and Space Science Institute, Daejeon, South Korea, Professor at the Korea University of Science

and Technology, Daejeon, South Korea, and Research Fellow at the Center for Space Research of the University of Texas at Austin, Austin, TX, USA. He is currently a Professor with the Shanghai Astronomical Observatory, Chinese Academy of Sciences, Shanghai, China, and the Director of the Center for Space Geodesy, University of Mining and Technology, Xuzhou, China. His main research areas include satellite navigation, remote sensing, satellite gravimetry, and space/planetary sensing as well as soft/hardware development for wide applications.

Dr. Jin has been the President of the International Association of Planetary Sciences (2013–2015), President of the International Association of Geodesy Sub-Commission 2.6 (2011–2015), Editor-in-Chief of the *International Journal of Geoscience* (since 2010), Associate Editor-in-Chief of *Satellite Navigation* (since 2013), Associate Editor of *Advances in Space Research* (since 2013), and an editorial board member of other five international journals.



Liang Chang was born in Jingzhou, China, in 1984. He received the B.Eng. degree in surveying and mapping engineering from the Nanjing University of Technology, Nanjing, China, in 2006 and the Ph.D. degree in geodesy and surveying engineering from Hohai University, Nanjing, China, in 2011.

From July 2011 to May 2013, he was a Postdoctoral Fellow in the Shanghai Astronomical Observatory, Chinese Academy of Sciences, Shanghai, China. He is currently a Lecturer with the College of Marine Sciences, Shanghai Ocean University,

Shanghai, China. His research interests include synthetic aperture radar interferometry and ocean remote sensing.



Xiufeng He received the B.Eng. and M.S. degrees in control and navigation from the Nanjing University of Aeronautics and Astronautics, Nanjing, China, in 1986 and 1989, respectively, and Ph.D. degree in navigation and survey engineering from Hong Kong Polytechnic University, Hong Kong, in 1998.

In the period of 1998–1999, she was a Postdoctoral Fellow at the Norwegian University of Science and Technology in Trondheim, Norway, where she was working in guidance, navigation, and control.

She worked at the Global Positioning System (GPS) Center, Singapore Nanyang Technological University, Singapore, in 2000 as a Research Fellow. She is currently a Professor and the Director of the Institute of Satellite Navigation and Spatial Information, Hohai University, Nanjing, China. Her main research interests include interferometric synthetic aperture radar, global navigation satellite system (GPS and GLObal NAVigation Satellite System), inertial navigation system (INS), and the low-cost integrated GNSS/INS navigation system. She has published three books and over 130 referred papers.